The structure of composite volcanoes unravelled by analogue modeling: a review

Lucie MATHIEU[a,*]

[a]**L. Mathieu.** Centre d'études sur les Ressources minérales (CERM), DSA (Département des Sciences Appliquées), Université du Québec à Chicoutimi (UQAC), 555 boul. de l'Université, Chicoutimi, Canada, G7H 2B1

***Corresponding author:** Lucie Mathieu (e-mail: lucie1.mathieu@uqac.ca; tel: (+001)-418-545-5011 ext. 2538)

Keywords: analogue models, volcano, regional faults, magma intrusions, surface deformation, spreading

Abstract :

Volcanic edifices are unstable accumulations of eruptive and intrusive products with complex internal structures. A documentation of these structures facilitates the assessing of the various hazards associated with volcanoes, e.g. flanks instabilities and eruptive events. However, structures are not easily assessed in the field, as volcanoes are regularly covered by eruptive products and are rapidly eroded. In the case of recent and active volcanoes, internal structures are generally extrapolated from the external morphology of the edifice, which can be documented using Digital Elevation Models (DEM) and geodetic data. Interpretation of such data greatly benefits from analogue models, which are idealised representations of reality used to test the impact that various processes may have on the shape of a volcanic edifice. This short review focuses on the contribution of analogue models to our comprehension of the internal structure of composite volcanic cones. The other volcanic morphologies (e.g. caldera) are excluded from this review, as they have distinct structure and evolution that have already been thoroughly reviewed. The reviewed models were used to investigate the impact that regional faults, magma injections and ductile substratum, among other processes, have on the internal structure and surface morphology of many volcanic edifices. These models were also used to locate unstable flanks and eruption sites.

1. Introduction

Volcanic edifices are unstable piles of generally un-coherent material regularly intruded by magma. The internal structure of volcanic cones is hard to assess, as the construction phase can be complex even in the smallest edifices (Delcamp et al., 2014) and the surface expression of faults and fractures is rapidly eroded and/or regularly covered by fresh eruptive products. Unrevealing the internal structure of volcanoes is however essential to assessing flank stability and the location of future eruptive events, and for a better comprehension of seismicity and overall deformation.

The structure of a volcano can be assessed in the field (Mathieu et al., 2011a) and with geophysical methods (Barde-Cabusson et al., 2012), but the most pertinent data, in the case of recent and active volcanoes, are generally obtained from the edifice morphology, an information that can be represented by Digital Elevation Models (DEM) (Grosse et al., 2014b). However, to relate the shape of a volcano to construction, intrusion, erosion and deformation events, the impact that each of these processes has on the geometry of a volcanic cone needs to be evaluated. This can be done using idealised representations such as numerical or analogue models. This short review focuses on the contribution of analogue models to our comprehension of the structure of composite volcanic cones. The other volcanic manifestations, such as monogenic cones, domes, mid-oceanic ridges, maar and calderas, are excluded from this review because they have distinct structure and evolution. The structure of calderas has also already been thoroughly reviewed (Cole et al., 2005; Acocella, 2008).

An analogue, or physical, model is a scaled simulation of natural processes (Acocella, 2008) with geometry, kinematic and dynamic similar to nature (Hubbert,

1937; Ramberg, 1981). Such models mostly enable a qualitative understanding of geologic processes. Their main advantage is to enable a visualisation of the structures that could arise as a result of progressive deformation (Hubbert, 1937; Ramberg, 1981). Their advantage over numerical simulations is to allow for discontinuous solutions, which can be difficult to obtain numerically (e.g. Holohan et al., 2011), while numerical models are more adapted to problems that necessitate a quantitative solution.

These last few decades, analogue models helped relate surface deformations to intrusive events, for example, or pointed to the flanks that may become unstable in response to movement along regional faults (Donnadieu and Merle, 1998; Grosse et al., 2009; Mathieu et al., 2011b). These models, which are reviewed here with special reference to composite cones, have provided the key observations that enable a comprehension of the internal structure and stability of natural volcanic edifices.

2. Analogue models

This section provides an overview of the materials and experimental setups most commonly used to simulate volcanic edifices.

2.1. Material and scaling

Scaling is performed to constrain the size of the analogue model (Hubbert, 1937; Sanford, 1959; Tibaldi, 1995). In this section, we use the upper crust to illustrate the scaling procedure. The brittle crust is generally modelled with sand, plaster, flour, clay, or a mixture of these materials. For such models, the length ratio L* (with L* = length in model / length in nature) is generally 10^{-5} and the gravity ratio g* is 1, except for centrifuge models (Dixon and Simpson, 1987). With g* equal 1 and a density ratio ρ* of

80 0.5, the stress ratio σ* (Eq. 1) is about 5.10^{-6} in this example (Merle and Vendeville,
81 1995).

82 $$\sigma^* = \rho^* g^* L^* \quad (1)$$

83 If we assume a cohesion of 10^7 Pa for natural rocks and as cohesion has the
84 dimension of stress ($c^* = \sigma^*$), the analogue material must have a cohesion of 50 Pa
85 (Merle and Vendeville, 1995). Sand is thus a good analogue for the upper crust because
86 its cohesion is negligible and its angle of internal friction is similar to this of brittle rocks.

87 Sand can also be mixed with about 10% flour or plaster to enhance the resolution
88 and details of the structures that develop at the surface of the model, but using such
89 mixture may increase the cohesion of the analogue material to unacceptable levels.
90 Alternatively, sand models can be dusted with plaster to enhance surface resolution. The
91 main disadvantage of sand is that water injections used as mafic intrusions analogues
92 (Kennedy et al., 2004) will wet this granular material instead of propagating as dykes and
93 sills. To address this issue, the crust can be modelled by gelatine, which has the
94 advantage of failing in tension (Kavanagh et al., 2013). However, gelatine has an
95 elevated cohesion and necessitates that the L* parameter be increased; i.e. models will
96 represent smaller portions of the crust.

97 To model magma injections, another alternative is to use a material that allows for
98 the circulation of low viscosity fluids, such as fine-grained powder of crystalline silica
99 (grain size about 15 μm) (Galland et al., 2007), a mixture of silica sand and crushed silica
100 powder (Norini and Acocella, 2011), or a sieved ignimbrite deposit (Mathieu et al.,
101 2008). These materials have however elevated cohesion and angle of internal friction
102 compared to sand.

Magma analogues, on the other hand, can correspond to water as well as air (Marti et al., 1994; Acocella and Tibaldi, 2005; Tibaldi et al., 2014), Golden Syrup, honey (Mathieu et al., 2008), vegetable oil (Galland et al., 2007), and silicone (Roche et al., 2000). Many silicone products with various viscosity are available on the market, and silicone-sand mixtures can also be used to adjust the viscosity to fulfil scaling requirements (for a discussion on silicone rheology, see Weijermars et al., 1993; Hailemariam and Mulugeta, 1998). The viscosity of the other materials can be adjusted through heating. A variety of material can thus be used to simulate magma, whose viscosity can vary over 12 orders of magnitudes in nature (Talbot, 1999).

The appropriate material is selected once the viscosity ratio μ^*, which is related to the strain ratio ε^*, is adjusted (see time ratio t^*; Eq. 2).

$$t^* = 1/\varepsilon^* = \mu^*/\sigma^* \quad (2)$$

These parameters are related to the injection rate of the analogue magma v^* ($v^* = \varepsilon^* L^*$) (Merle and Vendeville, 1995). The μ^* parameter is adjusted so that the experiment can run within a reasonable time span, and the magma analogue is selected accordingly.

In general, air or water are good analogues of basaltic magma and can be injected in gelatine to simulate dykes (Tibaldi et al., 2014). In granular material, however, air and water must be confined inside a balloon and simulate inflating or deflating magma chambers. Heated vegetable oil, on the other hand, can be injected in granular materials. This material has a low viscosity and is also a good analogue of basaltic magma. Vegetable oil has the advantage to solidify at room temperature, enabling the excavation and study of the shape of the injection (Galland et al., 2007). To obtain a similar result with the more viscous honey and Golden Syrup, which are analogue for mafic to felsic

126 magmas, the model is placed in a freezer (Mathieu et al., 2008). Viscous felsic magmas
127 can be modelled using silicone, which is also a good analogue of the lower crust and of
128 weak horizons of the upper crust (e.g. unconsolidated sediments, clays, evaporite).
129
130 **2.2. Experimental setup**
131 A commonly used experimental setup consists in a wood box with moving walls
132 connected to a motor (to simulate regional compression or else), filled with sand (upper
133 crust analogue) of divers colours (marker horizons) and with a pierced floor to allow for
134 the injection of a magma analogue. During an experiment, structures developing at the
135 surface of the model are photographed. Vertical structures can be observed behind a glass
136 (Le Corvec and Walter, 2009) or are recorded once the experiment is completed, by
137 slicing the model that has previously been consolidated by a mixture of soap and water
138 (Merle and Vendeville, 1995).
139 To follow the horizontal displacement at the surface of the model, or to follow
140 vertical displacements for models performed behind a glass, data are recorded by time-
141 lapse photography. These data are then analysed by a software that matches particles
142 from a picture to the next, thus following their displacements and producing horizontal or
143 vertical velocity maps (Burchardt and Walter, 2010; Walter, 2011). Surface geometries
144 can also be examined using DEM produced from 3D photogrammetry (Cecchi et al.,
145 2003, 2004; Donnadieu et al., 2003; Delcamp et al., 2008; Galland et al., 2016), laser
146 scanner data (Norini and Acocella, 2011), or the Kinect system (Tortini et al., 2014). The
147 experimental results are then compared to natural examples using these qualitative

148 observations (e.g. shape and distribution of faults) as well as dimensionless numbers (e.g.
149 cone height / diameter).
150
151 **3. Experimental studies of volcanoes**
152 Analogue models have been used to comprehend the interaction between volcanoes
153 and regional faults, the deformation induced by magma injections, and many other
154 processes that impact on the structure of volcanoes. This section reviews models of the
155 morphology and internal structure of composite volcanic cones that were mostly used to
156 infer the location of unstable flanks and/or eruptions.
157 **3.1. Location of volcanoes**
158 Volcanoes form where a magma supply is available. The location of individual
159 edifices is also dependent on the stress field and structure of the crust. In brittle rocks,
160 magma is mostly transported by dykes that orient parallel to the main horizontal stress
161 and/or infiltrate pre-existing structures (Tibaldi, 2004; Tibaldi et al., 2009; Bonali et al.,
162 2011; Mathieu et al., 2015), as indicated by the many analogue and numerical models
163 used to document the mechanism of dyke propagation (Hyndman and Alt, 1987; Galland
164 et al., 2006; Mathieu et al., 2008; Rivalta et al., 2015). Numerical models have also
165 shown that dykes can be "captured" by active faults and may impact on the kinematic of
166 these structures (Gaffney et al., 2007).
167 The study of natural examples indicates that extensional settings promote the raise
168 of magma in the crust, and that the intersection between pre-existing fractures, normal
169 and/or strike-slip faults, focalizes magmatic activity and promotes the construction of
170 volcanic cones (e.g. Guadeloupe volcanoes; Fig. 1a) (Tibaldi, 1992; Feuillet et al., 2002;

171 Abebe et al., 2007). Magma may also raise to the surface in compressional settings, as
172 was shown by vegetable oil injected in silica powder within a box subjected to horizontal
173 shortening (Galland et al., 2007). In these models, the analogue magma first propagates
174 as a sill at the base of the experimental setup, then thrust faults nucleate at the edge of the
175 sill to eventually channel the oil toward the surface. These models were compared to
176 Andean volcanoes formed in active compressional settings. Also, the modelled thrust
177 fault infiltrated by magma becomes arcuate, indicating that the geometry of regional
178 faults can be modified by magma intrusions (Fig. 1b) (Galland et al., 2007).
179
180 **3.2. Eruptive products and intrusions**
181 Volcanic cones can be viewed as unstable piles of eruptive products. Using
182 stratified cones made of intercalated layers of sand and sand-flour mixtures, it was shown
183 that stratification in a deformed cone promotes superficial and relatively small-volume
184 collapses and may limit large-volume catastrophic collapses (Fig. 2a) (Donnadieu and
185 Merle, 1998). Other models consisting of a sand cone containing an inflating balloon
186 were used to relate flank instabilities to multiple dyke injections. The results show that
187 multiple dyke injections can trigger small landslides on the volcano flanks perpendicular
188 to the strike of the dyke swarm, and much larger landslides along the volcano flanks
189 parallel to the dykes (Tibaldi et al., 2010). Other experimental results were used to
190 propose that accumulating eruptive products cause the constant creep observed over the
191 flank of the Stromboli volcano, Italy, and that magma injections accelerate these
192 movements and promote flank failure (Nolesini et al., 2013).

193 A large proportion of the volume of a volcanic cone is made of intrusions. Several
194 analogue models were used to demonstrate that intrusive events can strongly modify the
195 internal structure of an edifice. For example, silicone injected in a sand cone was used to
196 model the triggering mechanism of the 1980's sector collapse of Mount St-Helens
197 volcano, United-States of America (Donnadieu and Merle, 1998). The injected analogue
198 magma induced summit extension and a bulge delimited by a reverse fault on one flank
199 of the cone. This bulge is an analogue for potentially large-volume sector collapse in
200 nature (Fig. 2a) (Donnadieu and Merle, 1998). On other volcanoes, the summit extension
201 induced by the injection of a large volume of magma may take the shape of a depression
202 called a "crater of elevation" (Wyk de Vries et al., 2014). Such magma injection may
203 induce uplift, modify the internal structure of a volcano and impair its stability. Analogue
204 models can be used to model the surface expression of intrusions and to estimate the
205 shape of natural magma accumulations (Wyk de Vries et al., 2014) (Fig. 2b).
206 The load of a volcanic cone can also influence the propagation of magma in the
207 crust (Gaffney and Damjanac, 2006) as was shown using gelatine and sand box models
208 (Kervyn et al., 2009). Such models were used to propose that fresh magma injections can
209 be diverted from the summit of a volcanic cone in closed-conduit situations. These
210 intrusions may induce eruptions at the base of the edifice or along break-in-slopes on the
211 flanks of the volcano (Fig. 2c) (Kervyn et al., 2009). Magma propagation in a volcanic
212 cone is also strongly dependent on the structure of the edifice and may be influenced by
213 the regional stress field, as was shown using gelatine models (Pasquaré and Tibaldi,
214 2003). Analogue models have been used to explore many other aspects of the propagation

of magma in volcanic cones, and the reader interested by volcano plumbing systems is referred to recent reviews on this topic (Galland et al., 2015; Tibaldi, 2015).

3.3. Volcanic cones and regional faults

Where magma is channelled by an active fault, movement along this underlying regional structure will have a strong impact on the internal structure of the volcanic edifice. For example, for cones built in extensional settings over two normal faults (i.e. rift zone), models show that a curved graben will develop in the cone if its diameter is superior to the thickness of the rift zone (Fig. 3a) (van Wyk de Vries and Merle, 1996). Other volcanoes may be underlain by one or two intersecting normal faults, as was modelled using sand cones. In these experiments, normal fault motion induces summit subsidence delimited by a normal fault on one flank of the sand cone and a reverse fault on the opposite flank (Fig. 3b) (Vidal and Merle, 2000; Merle et al., 2001). The reverse fault delimits a bulged area; i.e. an unstable flank in nature (Vidal and Merle, 2000; Merle et al., 2001). Similar results are obtained with curved normal faults, which are analogue for the ring faults formed by the collapse of a caldera (Belousov et al., 2005). These analogue models also indicate that regional extension may form a symmetrical graben in a volcanic edifice, which may promote open conduit eruptions along a volcanic rift zone. Such edifices may be relatively stable (Fig. 3a). On the other hand, volcanoes located on a single active normal fault are more susceptible to large-volume sector collapses (Fig. 3b).

The impact that extensional stress fields have on the structure of volcanic cones have also been modelled using sand cones and numerical simulations (Cailleau et al.,

2003). The experimental results indicate that extension combined with balloon deflation (i.e. analogue for a subsiding magma chamber) reproduces the enigmatic structures observed on Mars volcanoes; i.e. linear extensional structures that become increasingly concentric in volcanic edifices (Fig. 3c) (Cailleau et al., 2003).

The geometry of regional faults can also be influenced by the development of volcanic cones, as was shown by analogue models consisting of a sand layer overlain by a sand cone and subjected to extension by separating plates located at the base of the experimental setup (van Wyk de Vries and Merle, 1996). By introducing an offset between the rift axis and the summit of the modelled cone, it was shown that the load of the sand cone can modify the orientation of the regional normal faults (Fig. 3e) (van Wyk de Vries and Merle, 1996).

For volcanoes built on active reverse faults, they may develop an apical graben and a reverse fault delimiting a bulged area according to sand cone models (Fig. 3e). The geometry of these faults was documented in details by progressively offsetting the sand cone from the regional reverse fault (Tibaldi, 2008). Also, it was proposed that the summit graben may favour the raise of magma in the volcano and that such intrusions may push the bulged and unstable flank outward and promote flank instabilities (Fig. 3e) (Tibaldi, 2008). Sand models were also used to study the effect that a variety of faults have on the structure of volcanic cones. Experimental results were used to relate the location and potential volume of sector collapses to the dip and kinematic of the investigated faults (Wooller et al., 2009).

Other models were used to document the complex fault pattern that develop in volcanic cones interacting with active strike-slip faults. In such context, a summit graben

is observed, as well as sigmoidal faults defining a flower structure inside the cone and a combination of reverse and normal faults over its flanks (Fig. 3f) (Lagmay et al., 2000). Additional sand models were used to propose that an active volcano may look perfectly symmetrical on the outside while having a strongly fractured internal structure (Norini and Lagmay, 2005). Bulged area, which are analogue of potential sector collapses, are also identified along the modelled reverse to transpressional flank faults (Fig. 3f) (Norini and Lagmay, 2005). Similar results were obtained by modelling the effect that transpressional and transtensional movements along regional faults have on the structure of sand cones (Fig. 3g, h) (Mathieu and van Wyk de Vries, 2011).

3.4. Spreading

3.4.1. Spreading and ductile substratum

Once a volcanic edifice reaches a sufficient volume, it may "sink" or "spread" over its weak substratum. For example, the load of the largest Earth volcano, Hawaii, has bent the underlying oceanic crust and is a classic example of sagging (Byrne et al., 2013). The internal structure of sagging volcanoes was investigated using sand and plaster cones built over a thick silicone layer that is an analogue for the ductile crust. In such models, a distal concentric graben and a flexural trough are observed around the base of the sand cone, and delicate convex structures, called terraces, are observed on the flanks of the cone (Fig. 4a, b) (Kervyn et al., 2010; Byrne et al., 2015). The terraces correspond to the surface expression of inward-dipping reverse faults, and their development is enhanced when the thickness of the ductile crust is reduced. These terraces are similar to the enigmatic structures observed on the flanks of the giant sagging Olympus Mount volcano

284 on Mars (Byrne et al., 2015). A continuum between sagging and spreading has also been
285 documented using ductile layers of variable thicknesses (Fig. 4a, b, c, d) (Byrne et al.,
286 2013).

287 Using similar experimental setups, it was observed that sand cones spread if the
288 thickness of the underlying silicone layer is inferior to the height of the volcanic cone
289 (Delcamp et al., 2008; Kervyn et al., 2010). In nature, thin weak horizons may
290 correspond to unconsolidated sediments and volcanoclastic deposits altered by magmatic
291 and other fluids. These horizons are located at the base of the edifice (e.g. marine
292 deposits) or inside the volcano (e.g. hyaloclastites accumulated on top of an emerging sea
293 volcano; see next section). Also according to observations made on natural volcanoes,
294 spreading is a slow process that increases the diameter of a volcanic cone while
295 decreasing its height. Ultimately, spreading stabilises an edifice but during spreading, a
296 volcano may have unstable flanks (van Wyk de Vries and Matela, 1998; Borgia et al.,
297 2014). Models consisting of sand cones built over thin silicone layers confirm these
298 observations and indicate that spreading induces extension in the upper part of the cone
299 and compression at its base, and initiates only if the basement contains a shallow ductile
300 layer of sufficient thickness (Merle and Borgia, 1996). Spreading also forms concentric
301 "leaf grabens" on the flanks of the edifice and folds and thrusts at its base (Fig. 4c, d)
302 (Merle and Borgia, 1996; Borgia et al., 2000; Kervyn et al., 2010).

303 Using similar models, several dimensionless numbers (e.g. volcano height/radius)
304 were proposed. These numbers can be applied to natural volcanoes to estimate the
305 advancement of spreading and its impact on flank stability (Borgia et al., 2000).
306 Qualitative observations were also made on the spreading-related structures. For

example, grabens are more abundant on steep cones or on cones located over the thinnest ductile layers (Delcamp et al., 2008). Also, the normal faults of the "leaf grabens" may accommodate strike-slip motions and delimit unstable flanks. These instabilities were investigated using silicone layers with limited extent that are analogues for the hydrothermally altered base of oceanic island volcanoes (Fig. 4c) (Delcamp et al., 2008). Analogue models can also be modified to fit the geometry of particular volcanoes. For example, the laterally spreading long flanks of the elongated Mount Cameroon, Cameroon, maintain a steep slope, while the slope of spreading flanks generally tends to decrease. This particular configuration was explained using elongated sand cones sitting on silicone layers with variable thicknesses (Fig. 4e) (Kervyn et al., 2014b). Overlapping cones of various ages are another peculiar volcanic geometry that can be easily modelled. Overlapping sand cones built over silicone layers were used to model linear extensional structures that may correspond to volcanic rift zones in nature (Walter et al., 2006).

The flank instabilities induced by spreading have been further investigated by dedicated models. These instabilities are particularly pronounced for dipping ductile substratum. In such scenario, the downdip slope focuses lateral movements and has a large potential for deep-seated sector collapses (Fig. 5a) (Wooller et al., 2004). The largest collapse events may destroy most of the volcanic edifice and produce Debris Avalanche Deposits (DAD). Such events form an amphitheatre scare in the volcanic cone, "toreva" (giant) blocks, and a blocky deposit with a hummocky surface. These features were successfully reproduced by placing a horizontal silicone layer beneath one flank of a sand cone (Fig. 6). Such models were used to quantify horizontal movements in the different parts of the avalanche and to investigate the mechanism of formation of

330 DAD (Andrade and van Wyk de Vries, 2010) and hummocks (Paguican et al., 2014).
331 Additional sector collapse triggering factors were also investigated using analogue
332 models (Acocella, 2005).
333
334 **3.4.2. Weak core**
335 In addition to ductile substratum, volcanoes may contain weak areas capable of
336 inducing spreading in parts of the edifice. These weak areas may correspond to
337 hydrothermally altered cores that were modelled using sand cones containing a
338 rectangular silicone layer. Experimental results correspond to "pit collapse" (i.e. summit
339 depression) or symmetrical to asymmetrical flank spreading (i.e. potentially unstable
340 flanks), depending on the location of the silicone core (Cecchi et al., 2004). Similar
341 models were used to investigate the large depressions (i.e. hydrothermal calderas)
342 observed in the upper part of several composite volcanoes (Barde- Cabusson and Merle,
343 2007; Merle et al., 2010). It was shown that hydrothermal calderas form by ripening or
344 unbuttressing (Merle et al., 2010). Ripening initiates once a sufficient volume of rocks
345 has been hydrothermally altered, is triggered by summit loading, and induces summit
346 subsidence and lateral flank spreading. If the altered area is too close from the summit or
347 if the volcano has shallow flanks, then summit loading may be insufficient and the edifice
348 is stable. However, if a flank of the volcano loses material for some reasons (e.g. due to
349 collapse), then the weak core is no longer confined and lateral spreading may initiate.
350 This scenario corresponds to unbuttressing and is characterised by flank subsidence and
351 sliding (Merle et al., 2010)
352 In addition to hydrothermally altered rocks, volcanoes may contain weak areas such
353 as hyaloclastites and sedimentary horizons. Such rocks are particularly abundant in

354 volcanic islands, to which several analogue models are dedicated. These models consist
355 in sand cones built over a thin ductile layer (i.e. analogue of marine sediments,
356 hyaloclastites, or other ductile units) and containing an additional silicone layer (i.e.
357 analogue of the hyaloclastite layer developed at the water-atmosphere interface) or
358 several dipping silicone layers (i.e. analogue of paleodelta developed below the water-
359 atmosphere interface) (Oehler et al., 2005). These models were used to document
360 interfering lateral spreading movements and to evaluate their impact on flank stability
361 (Fig. 5b). For example, it was shown that basal spreading decreases the slope of the cone
362 and reduces the risk of collapse (Fig. 5c). When spreading over the basal layer is too slow
363 however, the ductile horizons located inside the cone may trigger large-volume sector
364 collapses (Fig. 5d, e). Such catastrophic events may have produce the abundant debris
365 flow deposits observed at the feet of oceanic volcanoes (Oehler et al., 2005).
366
367 **3.5. Combined processes**
368 Analogue models have also been designed to test the combined effect of the
369 processes described previously. Such models more closely represent natural examples, in
370 which independent processes are generally coeval.
371 Some models may combine regional faults movements to the deformation induced
372 by magma injections. Using a balloon inflated in a sand cone deformed by the movement
373 of a normal fault (Fig. 7a), it was shown that magma injection is the main triggering
374 factor of sector collapses (Tibaldi et al., 2006). Comparing these experimental results to
375 the Ollagüe volcano, Andes, indicates that previously collapsed areas are more sensitive
376 to further collapses (Tibaldi et al., 2006).

377 Other models may combine local (i.e. spreading-related) to regional extension. The
378 combination of these extensional events produces a complex fault pattern in a sand cone
379 (Fig. 7b) (van Wyk de Vries and Merle, 1996). Spreading can also be combined to strike-
380 slip, transpressional or transtensional motions along regional faults. These models
381 produce complex fault patterns and were used to document the location and volume of
382 potentially unstable flanks (Fig. 7c, d) (Mathieu and van Wyk de Vries, 2011; Mathieu et
383 al., 2011b).

384 Other models were used to document the interaction between intrusive events and
385 spreading movements. For example, Golden Syrup (i.e. magma analogue) injections were
386 performed beneath a granular cone sitting on a thin silicone layer to model the sub-
387 volcanic complex of the Mull volcano, Scotland (Mathieu and van Wyk de Vries, 2009).
388 The weak substratum underlying this volcano is too thin to induce spreading. However,
389 using the results of analogue modelling (Fig. 7e), it was shown that intrusive events may
390 induce lateral spreading of a part of the volcanic cone and extension in the opposite flank,
391 where subsequent magma injections will tend to focus (Mathieu and van Wyk de Vries,
392 2009). Relationship between spreading movements and magma intrusions was further
393 investigated by injecting Golden Syrup in a silicone layer underlying a sand cone (Fig.
394 7f). The surface expression of deformation is similar to spreading-related structures, but
395 the velocity of the lateral movements is greatly increased by the development of the sub-
396 volcanic complex (Delcamp et al., 2012a). Other models consisting in granular cones
397 sitting on silicone layers and subjected to silicone injections (i.e. analogue of magma
398 injections in a volcanic rift zone) were used to demonstrate that, during periods of dyke
399 injections, movements along the basal decollement (i.e. horizontal silicone layer) may

400 accelerate and lock movements along the spreading-related normal faults (Le Corvec and
401 Walter, 2009). Thus, in some cases, magma injections stabilise the spreading flanks.

402 More elaborate models have been designed to investigate the combined effect of
403 more than two processes. For example, flank instabilities at Mt Etna can be modelled
404 using stratified sand cones built over a dipping substratum affected by regional extension,
405 in which silicone (i.e. magma chamber analogue) and vegetable oil (i.e. dyke analogue)
406 are injected (Norini and Acocella, 2011). Such models were used to demonstrate that
407 magma injection is the prominent factor that promotes flank instabilities (Norini and
408 Acocella, 2011).

409

410 **4. Conclusions**

411 The morphology of recent volcanoes can be used to infer their internal structure
412 with the aid of DEM data, morphometric studies (Grosse et al., 2014a) and geodetic
413 investigations. Analogue models are idealised representations of natural geological
414 entities that enable a rapid and efficient testing of the impact that various processes may
415 have on the morphology of a volcano. Such models have been successfully used, for
416 example, to relate bulging to magma injections, or to link enigmatic "leaf grabens" and
417 terraces to, respectively, spreading and sagging processes. Analogue models have also
418 been intensely used to locate unstable flanks and to identify the main factors that promote
419 sector collapses. In addition to these qualitative observations, analogue models can be
420 used to quantify deformation patterns. Such patterns can then be compared to the
421 geodetic data acquired on natural volcanoes (Delcamp et al., 2012b; Johannessen, 2014).

422 Analogue modelling has thus played an important role in our comprehension of the
423 structure of volcanic edifices.
424
425 **Acknowledgments**
426 Many thanks to the reviewers A. Tibaldi and O. Merle, and to the editors I. Aslop
427 and J. Hippertt, whose comments helped to greatly improved this contribution. The
428 author wishes to address warm thanks to B. van Wyk de Vries for guiding her in the field
429 of volcano-tectonics. Warm thanks are also addressed to various collaborators that
430 intervened in the study of several volcanoes over the years, such as V.R. Troll, M.
431 Kervyn, S. Burchardt, and A. Delcamp.
432
433 **References**
434 Abebe, B., Acocella, V., Korme, T., Ayalew, D., 2007. Quaternary faulting and
435 volcanism in the Main Ethiopian Rift. Journal of African Earth Sciences 48, 115–
436 124.
437 Acocella, V., 2008. Structural development of calderas: a synthesis from analogue
438 experiments. Developments in Volcanology 10, 285–311.
439 Acocella, V., 2005. Modes of sector collapse of volcanic cones: Insights from analogue
440 experiments. Journal of Geophysical Research: Solid Earth 110.
441 Acocella, V., Tibaldi, A., 2005. Dike propagation driven by volcano collapse: a general
442 model tested at Stromboli, Italy. Geophysical Research Letters 32.
443 Andrade, S.D., van Wyk de Vries, B., 2010. Structural analysis of the early stages of
444 catastrophic stratovolcano flank-collapse using analogue models. Bulletin of

445 Volcanology 72, 771–789.
446 Barde-Cabusson, S., Finizola, A., Peltier, A., Chaput, M., Taquet, N., Dumont, S.,
447 Duputel, Z., Guy, A., Mathieu, L., Saumet, S., Sorbadère, F., Vieille, M., 2012.
448 Structural control of collapse events inferred by self-potential mapping on the Piton
449 de la Fournaise volcano (La Réunion Island). Journal of Volcanology and
450 Geothermal Research 209–210, 9–18.
451 https://doi.org/10.1016/j.jvolgeores.2011.09.014
452 Barde- Cabusson, S., Merle, O., 2007. From steep- slope volcano to flat caldera floor.
453 Geophysical Research Letters 34.
454 Belousov, A., Walter, T.R., Troll, V.R., 2005. Large-scale failures on domes and
455 stratocones situated on caldera ring faults: sand-box modeling of natural examples
456 from Kamchatka, Russia. Bulletin of Volcanology 67, 457–468.
457 Bonali, F.L., Corazzato, C., Tibaldi, A., 2011. Identifying rift zones on volcanoes: an
458 example from La Réunion island, Indian Ocean. Bulletin of Volcanology 73, 347–
459 366.
460 Borgia, A., Delaney, P.T., Denlinger, R.P., 2000. Spreading volcanoes. Annual Review
461 of Earth and Planetary Sciences 28, 539–570.
462 Borgia, A., Mazzoldi, A., Brunori, C.A., Allocca, C., Delcroix, C., Micheli, L.,
463 Vercellino, A., Grieco, G., 2014. Volcanic spreading forcing and feedback in
464 geothermal reservoir development, Amiata Volcano, Italia. Journal of Volcanology
465 and Geothermal Research 284, 16–31.
466 Burchardt, S., Walter, T.R., 2010. Propagation, linkage, and interaction of caldera ring-
467 faults: comparison between analogue experiments and caldera collapse at

468 Miyakejima, Japan, in 2000. Bulletin of Volcanology 72, 297–308.
469 Byrne, P.K., Holohan, E.P., Kervyn, M., van Wyk de Vries, B., Troll, V.R., 2015.
470 Analogue modelling of volcano flank terrace formation on Mars. Geological
471 Society, London, Special Publications 401, 185–202.
472 Byrne, P.K., Holohan, E.P., Kervyn, M., van Wyk de Vries, B., Troll, V.R., Murray, J.B.,
473 2013. A sagging-spreading continuum of large volcano structure. Geology 41, 339–
474 342.
475 Cailleau, B., Walter, T.R., Janle, P., Hauber, E., 2003. Modeling volcanic deformation in
476 a regional stress field: Implications for the formation of graben structures on Alba
477 Patera, Mars. Journal of Geophysical Research: Planets 108, 5141.
478 https://doi.org/10.1029/2003JE002135
479 Cecchi, E., van Wyk de Vries, B., Lavest, J.-M., 2004. Flank spreading and collapse of
480 weak-cored volcanoes. Bulletin of Volcanology 67, 72–91.
481 Cecchi, E., van Wyk de Vries, B., Lavest, J.-M., Harris, A., Davies, M., 2003. N-view
482 reconstruction: a new method for morphological modelling and deformation
483 measurement in volcanology. Journal of Volcanology and Geothermal Research
484 123, 181–201.
485 Cole, J.W., Milner, D.M., Spinks, K.D., 2005. Calderas and caldera structures: a review.
486 Earth-Science Reviews 69, 1–26.
487 Delcamp, A., de Vries, B. van W., James, M.R., Gailler, L.S., Lebas, E., 2012a.
488 Relationships between volcano gravitational spreading and magma intrusion.
489 Bulletin of Volcanology 74, 743–765.
490 Delcamp, A., van Wyk de Vries, B., James, M.R., 2008. The influence of edifice slope

491 and substrata on volcano spreading. Journal of Volcanology and Geothermal
492 Research 177, 925–943.
493 Delcamp, A., van Wyk de Vries, B., James, M.R., Gailler, L.S., Lebas, E., 2012b.
494 Relationships between volcano gravitational spreading and magma intrusion.
495 Bulletin of Volcanology 74, 743–765.
496 Delcamp, A., van Wyk de Vries, B., Stéphane, P., Kervyn, M., 2014. Endogenous and
497 exogenous growth of the monogenetic Lemptegy volcano, Chaine des Puys, France.
498 Geosphere 10, 998–1019.
499 Dixon, J.M., Simpson, D.G., 1987. Centrifuge modelling of laccolith intrusion. Journal of
500 Structural Geology 9, 87–103.
501 Donnadieu, F., Kelfoun, K., van Wyk de Vries, B., Cecchi, E., Merle, O., 2003. Digital
502 photogrammetry as a tool in analogue modelling: applications to volcano instability.
503 Journal of Volcanology and Geothermal Research 123, 161–180.
504 Donnadieu, F., Merle, O., 1998. Experiments on the indentation process during
505 cryptodome intrusions: new insights into Mount St. Helens deformation. Geology
506 26, 79–82.
507 Feuillet, N., Manighetti, I., Tapponnier, P., Jacques, E., 2002. Arc parallel extension and
508 localization of volcanic complexes in Guadeloupe, Lesser Antilles. Journal of
509 Geophysical Research: Solid Earth 107.
510 Gaffney, E.S., Damjanac, B., 2006. Localization of volcanic activity: topographic effects
511 on dike propagation, eruption and conduit formation. Geophysical Research Letters
512 33.
513 Gaffney, E.S., Damjanac, B., Valentine, G.A., 2007. Localization of volcanic activity: 2.

514 Effects of pre-existing structure. Earth and Planetary Science Letters 263, 323–338.
515 Galland, O., Bertelsen, H.S., Guldstrand, F., Girod, L., Johannessen, R.F., Bjugger, F.,
516 Burchardt, S., Mair, K., 2016. Application of open source photogrammetric software
517 MicMac for monitoring surface deformation in laboratory models. Journal of
518 Geophysical Research: Solid Earth 121, 2852–2872.
519 Galland, O., Cobbold, P.R., de Bremond d'Ars, J., Hallot, E., 2007. Rise and
520 emplacement of magma during horizontal shortening of the brittle crust: Insights
521 from experimental modeling. Journal of Geophysical Research: Solid Earth 112.
522 Galland, O., Cobbold, P.R., Hallot, E., de Bremond d'Ars, J., Delavaud, G., 2006. Use of
523 vegetable oil and silica powder for scale modelling of magmatic intrusion in a
524 deforming brittle crust. Earth and Planetary Science Letters 243, 786–804.
525 Galland, O., Holohan, E., van Wyk de Vries, B., Burchardt, S., 2015. Laboratory
526 Modelling of Volcano Plumbing Systems: A Review. Advances in Volcanology.
527 Springer, 1–68. https://doi.org/10.1007/11157_2015_9
528 Grosse, P., de Vries, B. van W., Petrinovic, I.A., Euillades, P.A., Alvarado, G.E., 2009.
529 Morphometry and evolution of arc volcanoes. Geology 37, 651–654.
530 Grosse, P., Euillades, P.A., Euillades, L.D., de Vries, B. van W., 2014a. A global
531 database of composite volcano morphometry. Bulletin of Volcanology 76, 784.
532 Grosse, P., Euillades, P.A., Euillades, L.D., van Wyk de Vries, B., 2014b. A global
533 database of composite volcano morphometry. Bulletin of Volcanology 76, 784.
534 Hailemariam, H., Mulugeta, G., 1998. Temperature-dependent rheology of bouncing
535 putties used as rock analogs. Tectonophysics 294, 131–141.
536 Holohan, E.P., Schöpfer, M.P.J., Walsh, J.J., 2011. Mechanical and geometric controls on

537 the structural evolution of pit crater and caldera subsidence. Journal of Geophysical
538 Research: Solid Earth 116.
539 Hubbert, M.K., 1937. Theory of scale models as applied to the study of geologic
540 structures. Geological Society of America Bulletin 48, 1459–1520.
541 Hyndman, D.W., Alt, D., 1987. Radial dikes, laccoliths, and gelatin models. The Journal
542 of Geology 95, 763–774.
543 Johannessen, R.F., 2014. Laboratory Volcano Geodesy. University of Oslo.
544 Kavanagh, J.L., Menand, T., Daniels, K.A., 2013. Gelatine as a crustal analogue:
545 Determining elastic properties for modelling magmatic intrusions. Tectonophysics
546 582, 101–111.
547 Kennedy, B., Stix, J., Vallance, J.W., Lavallée, Y., Longpré, M.-A., 2004. Controls on
548 caldera structure: Results from analogue sandbox modeling. Geological Society of
549 America Bulletin 116, 515–524.
550 Kervyn, M., Boone, M.N., van Wyk de Vries, B., Lebas, E., Cnudde, V., Fontijn, K.,
551 Jacobs, P., 2010. 3D imaging of volcano gravitational deformation by computerized
552 X-ray micro-tomography. Geosphere 6, 482–498.
553 Kervyn, M., Ernst, G.G.J., van Wyk de Vries, B., Mathieu, L., Jacobs, P., 2009. Volcano
554 load control on dyke propagation and vent distribution: Insights from analogue
555 modeling. Journal of Geophysical Research 114, 26.
556 https://doi.org/10.1029/2008JB005653
557 Kervyn, M., van Wyk de Vries, B., Walter, T.R., Njome, M.S., Suh, C.E., Ernst, G.G.J.,
558 2014a. Directional flank spreading at Mount Cameroon volcano: Evidence from
559 analogue modeling. Journal of Geophysical Research: Solid Earth 119, 7542–7563.

560 Kervyn, M., Wyk de Vries, B., Walter, T.R., Njome, M.S., Suh, C.E., Ernst, G.G.J.,
561 2014b. Directional flank spreading at Mount Cameroon volcano: Evidence from
562 analogue modeling. Journal of Geophysical Research: Solid Earth 119, 7542–7563.
563 Lagmay, A.M.F., van Wyk de Vries, B., Kerle, N., Pyle, D.M., 2000. Volcano instability
564 induced by strike-slip faulting. Bulletin of Volcanology 62, 331–346.
565 Le Corvec, N., Walter, T.R., 2009. Volcano spreading and fault interaction influenced by
566 rift zone intrusions: Insights from analogue experiments analyzed with digital image
567 correlation technique. Journal of Volcanology and Geothermal Research 183, 170–
568 182.
569 Marti, J., Ablay, G.J., Redshaw, L.T. t, Sparks, R.S.J., 1994. Experimental studies of
570 collapse calderas. Journal of the Geological Society 151, 919–929.
571 Mathieu, L., Burchardt, S., Troll, V.R., Krumbholz, M., Delcamp, A., 2015. Geological
572 constraints on the dynamic emplacement of cone-sheets - The Ardnamurchan cone-
573 sheet swarm, NW Scotland. Journal of Structural Geology 80.
574 https://doi.org/10.1016/j.jsg.2015.08.012
575 Mathieu, L., Kervyn, M., Ernst, G.G.J., 2011a. Field evidence for flank instability, basal
576 spreading and volcano-tectonic interactions at Mt Cameroon, West Africa. Bulletin
577 of Volcanology 73. https://doi.org/10.1007/s00445-011-0458-z
578 Mathieu, L., van Wyk de Vries, B., 2011. The impact of strike-slip, transtensional and
579 transpressional fault zones on volcanoes. Part 1: Scaled experiments. Journal of
580 Structural Geology 33. https://doi.org/10.1016/j.jsg.2011.03.002
581 Mathieu, L., van Wyk de Vries, B., 2009. Edifice and substrata deformation induced by
582 intrusive complexes and gravitational loading in the Mull volcano (Scotland).

583 Bulletin of Volcanology 71. https://doi.org/10.1007/s00445-009-0295-5
584 Mathieu, L., van Wyk de Vries, B., Holohan, E.P., Troll, V.R., 2008. Dykes, cups,
585 saucers and sills: Analogue experiments on magma intrusion into brittle rocks. Earth
586 and Planetary Science Letters 271. https://doi.org/10.1016/j.epsl.2008.02.020
587 Mathieu, L., van Wyk de Vries, B., Pilato, M., Troll, V.R., 2011b. The interaction
588 between volcanoes and strike-slip, transtensional and transpressional fault zones:
589 Analogue models and natural examples. Journal of Structural Geology 33.
590 https://doi.org/10.1016/j.jsg.2011.03.003
591 Merle, O., Barde-Cabusson, S., de Vries, B. van W., 2010. Hydrothermal calderas.
592 Bulletin of Volcanology 72, 131–147.
593 Merle, O., Borgia, A., 1996. Scaled experiments of volcanic spreading. Journal of
594 Geophysical Research: Solid Earth 101, 13805–13817.
595 Merle, O., Vendeville, B., 1995. Experimental modelling of thin-skinned shortening
596 around magmatic intrusions. Bulletin of Volcanology 57, 33–43.
597 Merle, O., Vidal, N., van Wyk de Vries, B., 2001. Experiments on vertical basement fault
598 reactivation below volcanoes. Journal of Geophysical Research: Solid Earth 106,
599 2153–2162.
600 Nolesini, T., Di Traglia, F., Del Ventisette, C., Moretti, S., Casagli, N., 2013.
601 Deformations and slope instability on Stromboli volcano: Integration of GBInSAR
602 data and analog modeling. Geomorphology 180, 242–254.
603 Norini, G., Acocella, V., 2011. Analogue modeling of flank instability at Mount Etna:
604 understanding the driving factors. Journal of Geophysical Research: Solid Earth 116.
605 Norini, G., Lagmay, A.M.F., 2005. Deformed symmetrical volcanoes. Geology 33, 605–

608.

Oehler, J.-F., van Wyk de Vries, B., Labazuy, P., 2005. Landslides and spreading of oceanic hot-spot and arc shield volcanoes on Low Strength Layers (LSLs): an analogue modeling approach. Journal of Volcanology and Geothermal Research 144, 169–189.

Paguican, E.M.R., de Vries, B. van W., Lagmay, A.M.F., 2014. Hummocks: how they form and how they evolve in rockslide-debris avalanches. Landslides 11, 67–80.

Pasquaré, F.A., Tibaldi, A., 2003. Do transcurrent faults guide volcano growth? The case of NW Bicol Volcanic Arc, Luzon, Philippines. Terra Nova 15, 204–212.

Ramberg, H., 1981. Gravity, deformation, and the earth's crust: In theory, experiments, and geological application. Academic press, London.

Rivalta, E., Taisne, B., Bunger, A.P., Katz, R.F., 2015. A review of mechanical models of dike propagation: Schools of thought, results and future directions. Tectonophysics 638, 1–42.

Roche, O., Druitt, T.H., Merle, O., 2000. Experimental study of caldera formation. Journal of Geophysical Research: Solid Earth 105, 395–416.

Sanford, A.R., 1959. Analytical and experimental study of simple geologic structures. Geological Society of America Bulletin 70, 19–52.

Talbot, C.J., 1999. Can field data constrain rock viscosities? Journal of Structural Geology 21, 949–957.

Tibaldi, A., 2015. Structure of volcano plumbing systems: A review of multi-parametric effects. Journal of Volcanology and Geothermal Research 298, 85–135.

Tibaldi, A., 2008. Contractional tectonics and magma paths in volcanoes. Journal of

629 Volcanology and Geothermal Research 176, 291–301.
630 Tibaldi, A., 2004. Major changes in volcano behaviour after a sector collapse: insights
631 from Stromboli, Italy. Terra Nova 16, 2–8.
632 Tibaldi, A., 1995. Morphology of pyroclastic cones and tectonics. Journal of Geophysical
633 Research: Solid Earth 100, 24521–24535.
634 Tibaldi, A., 1992. The role of transcurrent intra- arc tectonics in the configuration of a
635 volcanic arc. Terra Nova 4, 567–577.
636 Tibaldi, A., Bistacchi, A., Pasquare, F.A., Vezzoli, L., 2006. Extensional tectonics and
637 volcano lateral collapses: insights from Ollagüe volcano (Chile- Bolivia) and
638 analogue modelling. Terra Nova 18, 282–289.
639 Tibaldi, A., Bonali, F.L., Corazzato, C., 2014. The diverging volcanic rift system.
640 Tectonophysics 611, 94–113.
641 Tibaldi, A., Corazzato, C., Marani, M., Gamberi, F., 2009. Subaerial-submarine evidence
642 of structures feeding magma to Stromboli Volcano, Italy, and relations with edifice
643 flank failure and creep. Tectonophysics 469, 112–136.
644 Tibaldi, A., Rust, D., Corazzato, C., Merri, A., 2010. Setting the scene for self-
645 destruction: From sheet intrusions to the structural evolution of rifted
646 stratovolcanoes. Geosphere 6, 189–210.
647 Tortini, R., Bonali, F.L., Corazzato, C., Carn, S.A., Tibaldi, A., 2014. An innovative
648 application of the Kinect in Earth sciences: quantifying deformation in analogue
649 modelling of volcanoes. Terra Nova 26, 273–281.
650 van Wyk de Vries, B., Màrquez, A., Herrera, R., Bruna, J.L.G., Llanes, P., Delcamp, A.,
651 2014. Craters of elevation revisited: forced-folds, bulging and uplift of volcanoes.

652 Bulletin of Volcanology 76, 875.
653 van Wyk de Vries, B., Matela, R., 1998. Styles of volcano-induced deformation:
654 numerical models of substratum flexure, spreading and extrusion. Journal of
655 Volcanology and Geothermal Research 81, 1–18.
656 van Wyk de Vries, B., Merle, O., 1996. The effect of volcanic constructs on rift fault
657 patterns. Geology 24, 643–646.
658 Vidal, N., Merle, O., 2000. Reactivation of basement faults beneath volcanoes: a new
659 model of flank collapse. Journal of Volcanology and Geothermal Research 99, 9–26.
660 Walter, T.R., 2011. Structural architecture of the 1980 Mount St. Helens collapse: An
661 analysis of the Rosenquist photo sequence using digital image correlation. Geology
662 39, 767–770.
663 Walter, T.R., Klugel, A., Munn, S., 2006. Gravitational spreading and formation of new
664 rift zones on overlapping volcanoes. Terra Nova 18, 26–33.
665 Weijermars, R., Jackson, M.P.A. t, Vendeville, B., 1993. Rheological and tectonic
666 modeling of salt provinces. Tectonophysics 217, 143–174.
667 Wooller, L., van Wyk de Vries, B., Cecchi, E., Rymer, H., 2009. Analogue models of the
668 effect of long-term basement fault movement on volcanic edifices. Bulletin of
669 Volcanology 71, 1111–1131.
670 Wooller, L., van Wyk de Vries, B., Murray, J.B., Rymer, H., Meyer, S., 2004. Volcano
671 spreading controlled by dipping substrata. Geology 32, 573–576.
672 Wyk de Vries, B., Màrquez, A., Herrera, R., Bruna, J.L.G., Llanes, P., Delcamp, A.,
673 2014. Craters of elevation revisited: forced-folds, bulging and uplift of volcanoes.
674 Bulletin of Volcanology 76, 875.

675

676

677

678 # Figure captions

679 **Fig. 1:** a) Structural setting of several Caribbean volcanoes (including the volcanoes of
680 the Guadeloupe island); and b) arcuate thrust developing in response to vegetable oil
681 injection in an analogue model. These drawings are inspired from (Feuillet et al., 2002;
682 Galland et al., 2007).

683 **Fig. 2:** Drawings inspired from: a) experimental results obtained with sand cones
684 destabilised by balloon inflation (Nolesini et al., 2013), silicone injection (Donnadieu and
685 Merle, 1998), and normal faulting (Vidal and Merle, 2000); b) interpretation of the
686 internal structure of the Puys de Dôme volcano, France (van Wyk de Vries et al., 2014);
687 and c) experimental results obtained by injecting various magma analogues in sand and
688 gelatine cones (Kervyn et al., 2009). For the legend, please refer to Fig. 1.

689 **Fig. 3:** Drawings inspired from experimental results obtained with sand cones
690 constructed: on the side (d) and over (a) the axis of a rift zone (van Wyk de Vries and
691 Merle, 1996); b) over a normal fault (Vidal and Merle, 2000; Merle et al., 2001); e) over
692 a reverse fault (Tibaldi, 2008); f) over a strike-slip fault (Lagmay et al., 2000; Norini and
693 Lagmay, 2005); and over transtensional (g) and transpressional (h) faults (Mathieu and
694 van Wyk de Vries, 2011). Drawing (c) of a cone subjected to extension, and inspired
695 from the combined results of numerical and analogue models (Cailleau et al., 2003). For
696 the legend, please refer to Fig. 1.

Fig. 4: Drawings inspired from experimental results obtained: in sagging (a) and sagging-spreading (b) sand cones (Kervyn et al., 2010; Byrne et al., 2015); c) in a sand cone spreading over a ductile layer with a limited extent (Delcamp et al., 2008); d) in sagging to spreading sand cones (Delcamp et al., 2008; Kervyn et al., 2010; Byrne et al., 2015); and e) in an elongated sand cone spreading over a ductile layer with a variable thickness (Kervyn et al., 2014a). For the legend and the scale, please refer to Fig. 1 and 3, respectively.

Fig. 5: Drawings inspired from experimental results obtained using: a) sand cones located over a dipping ductile substratum (Wooller et al., 2004); b, c, d, e) sand cones built over a ductile substratum (b, c), and containing a ductile layer (b, d) and/or dipping ductile layers (b, e) (Oehler et al., 2005). For the legend and the scale, please refer to Fig. 1 and 3, respectively.

Fig. 6: Drawing inspired from experimental results obtained using a sand cone partially underlain by a ductile layer (Andrade and van Wyk de Vries, 2010). For the legend and the scale, please refer to Fig. 1 and 3, respectively.

Fig. 7: Drawings inspired from experimental results obtained using sand cones sitting on brittle (a) or ductile (b, c, d, e, f) substratum, and subjected to: a) regional extension and balloon inflation (Tibaldi et al., 2006); b) regional extension (van Wyk de Vries and Merle, 1996); c-d) transtensional (c) and transpressional (d) fault movements (Mathieu and van Wyk de Vries, 2011); and e-f) Golden Syrup injections performed below (e) (Mathieu and van Wyk de Vries, 2009) or within (f) (Delcamp et al., 2012b) the ductile layer. For the legend and the scale, please refer to Fig. 1 and 3, respectively.

Figure 01

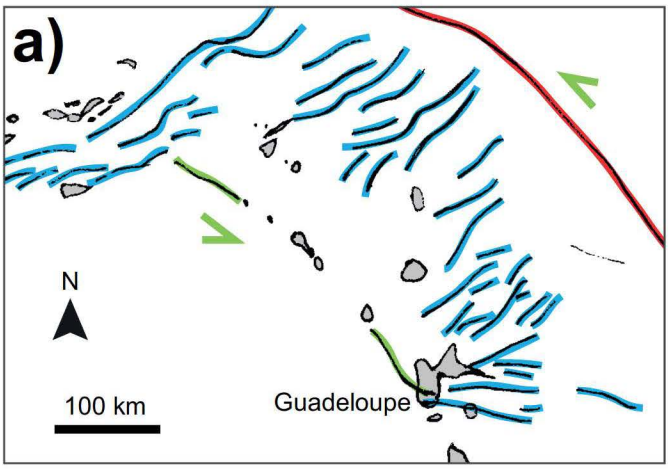

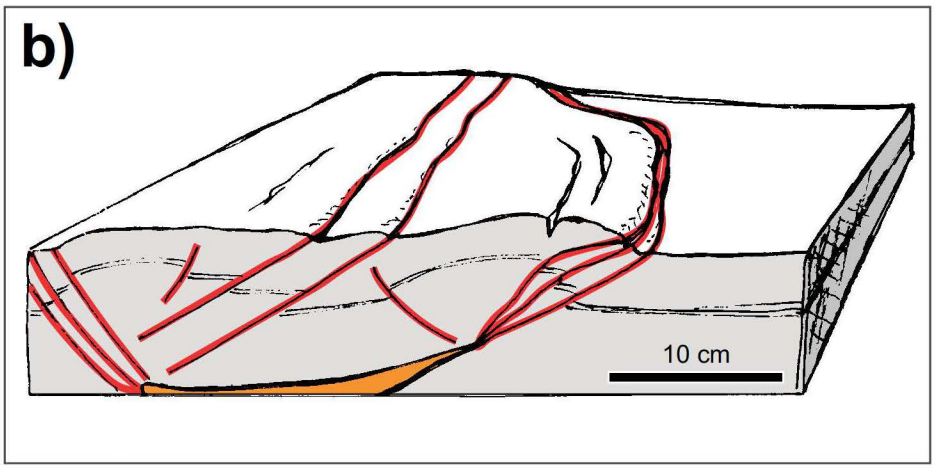

Legend

- Faults dominated by a normal component
- Faults dominated by a reverse component
- Faults dominated by a strike-slip component

Analogue model	Nature
Sand, plaster, silica powder, etc.	Brittle rocks (upper crust, volcano, etc.)
Silicone, silicone and sand mixture	Ductile rocks (ductile crust, sediments, etc.)
Air, water, vegetable oil, silicone, etc.	Mafic to felsic magmas
Bulged area, area moving outward	Potentially unstable flank

Figure 02

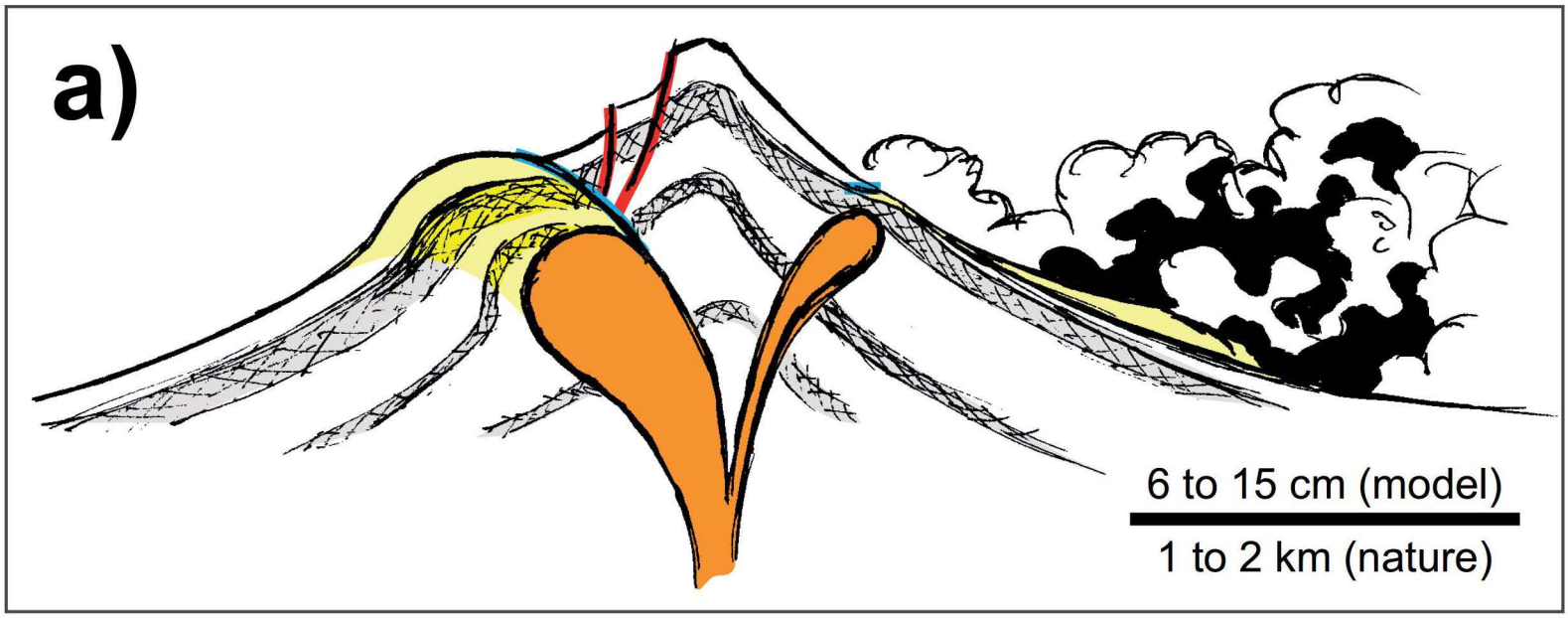

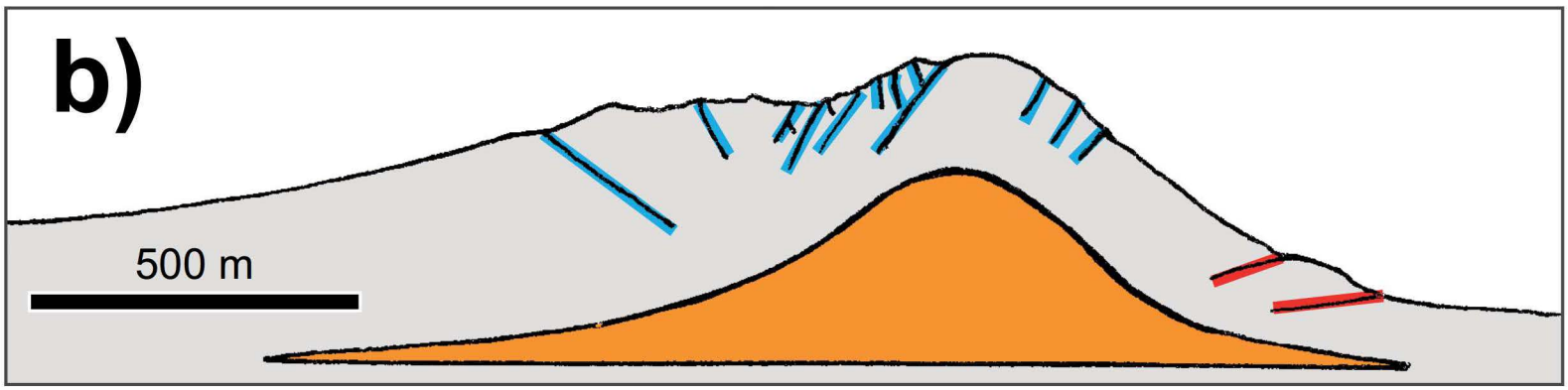

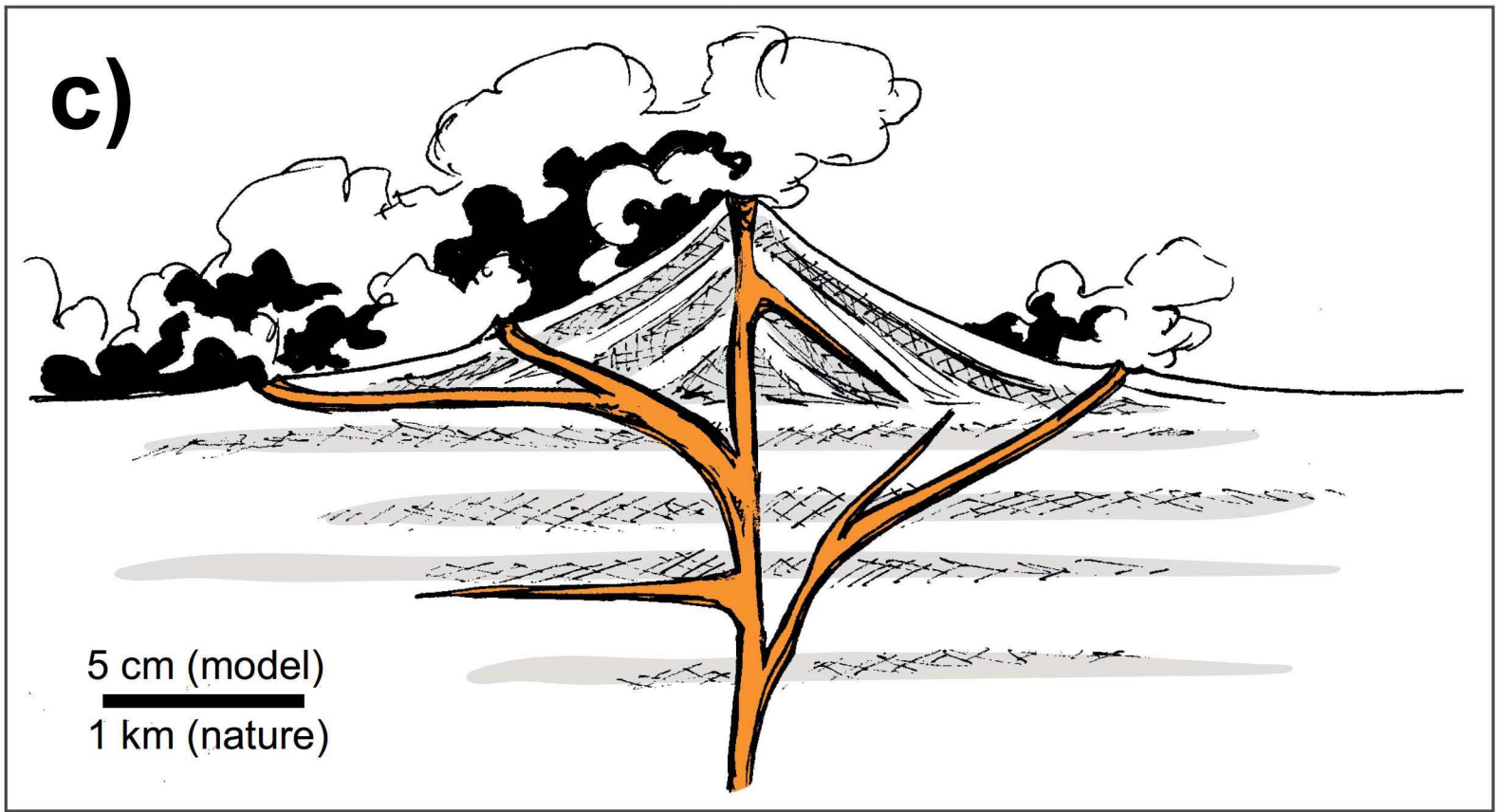

Figure 03

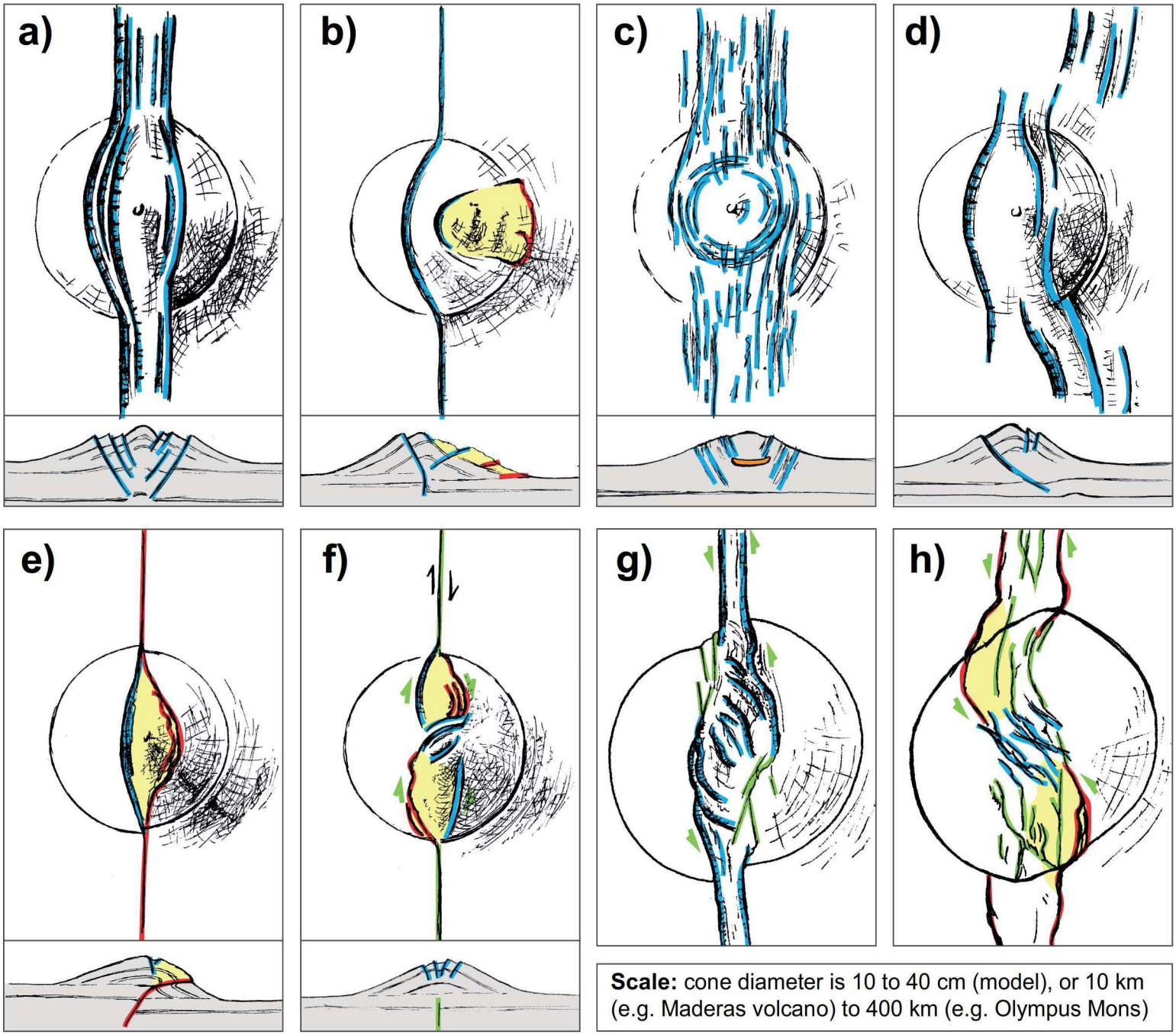
a)
b)
c)
d)
e)
f)
g)
h)
1
Scale: cone diameter is 10 to 40 cm (model), or 10 km (e.g. Maderas volcano) to 400 km (e.g. Olympus Mons)

Figure 04

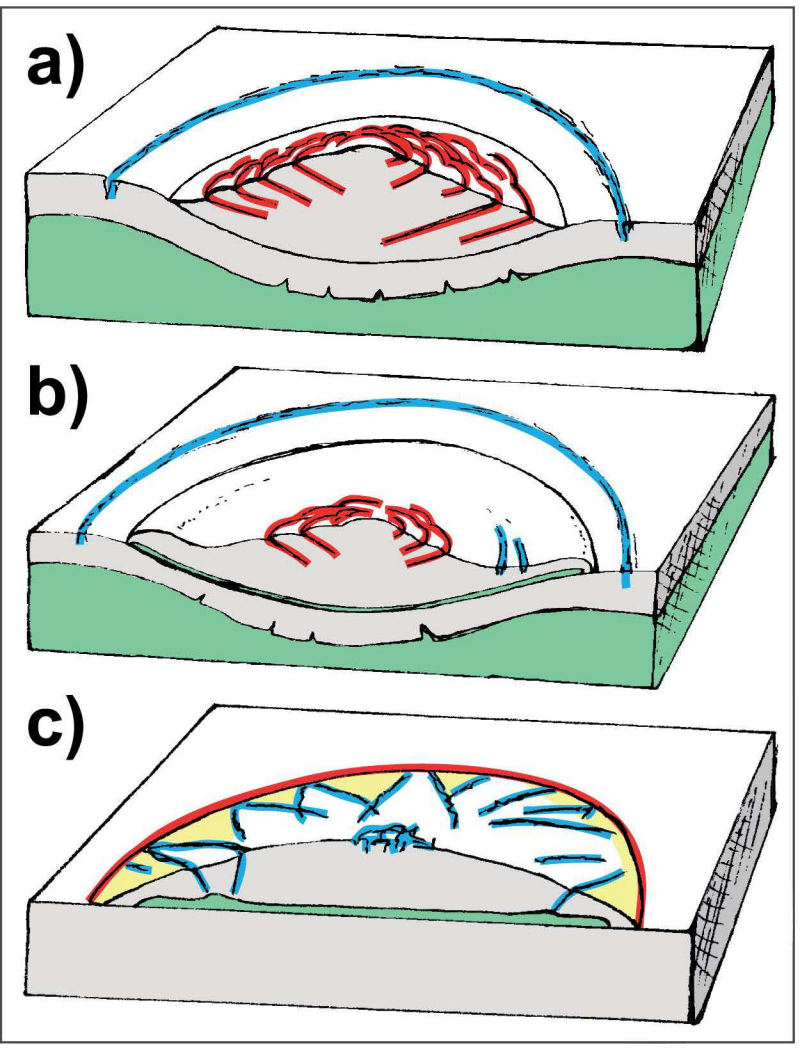

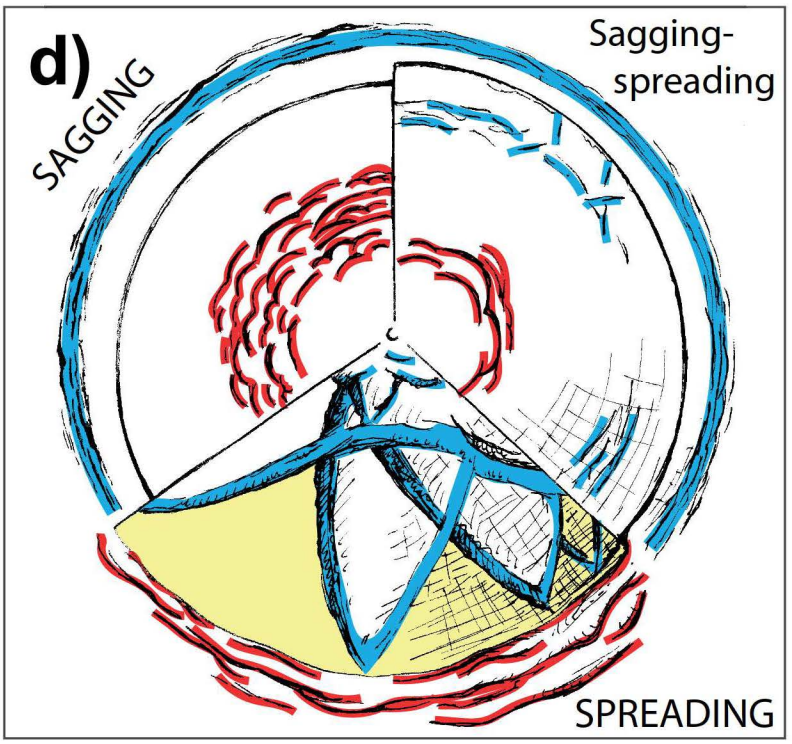

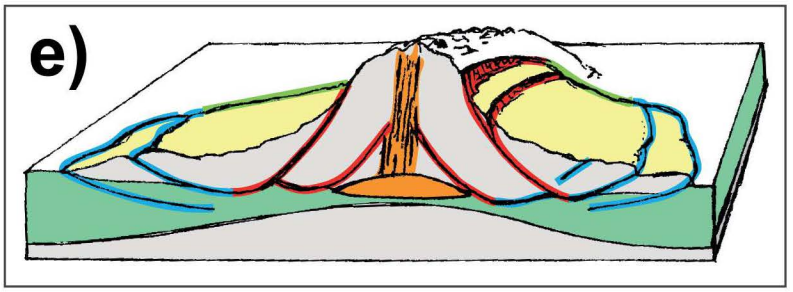

Figure 05

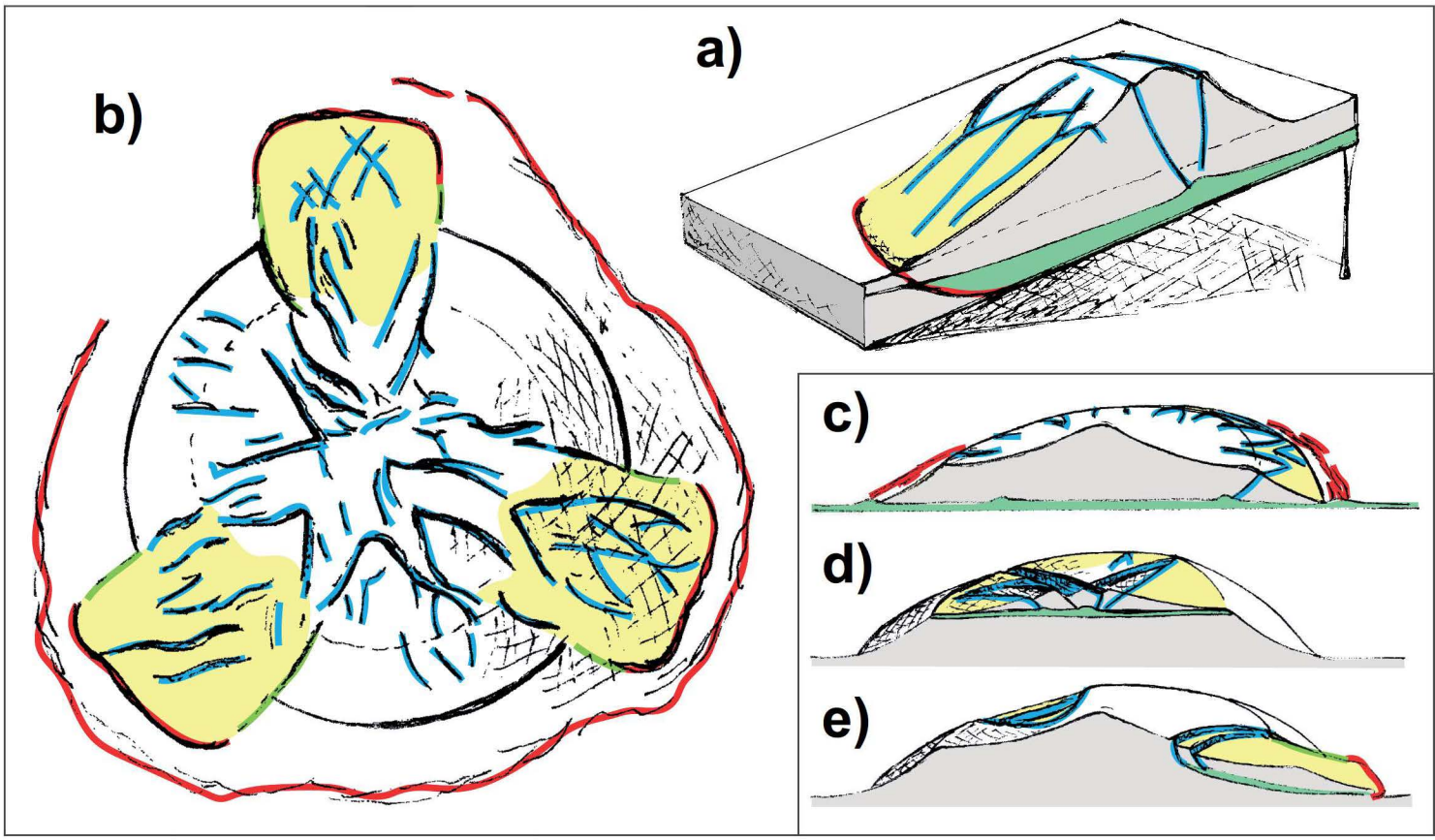

ure 06

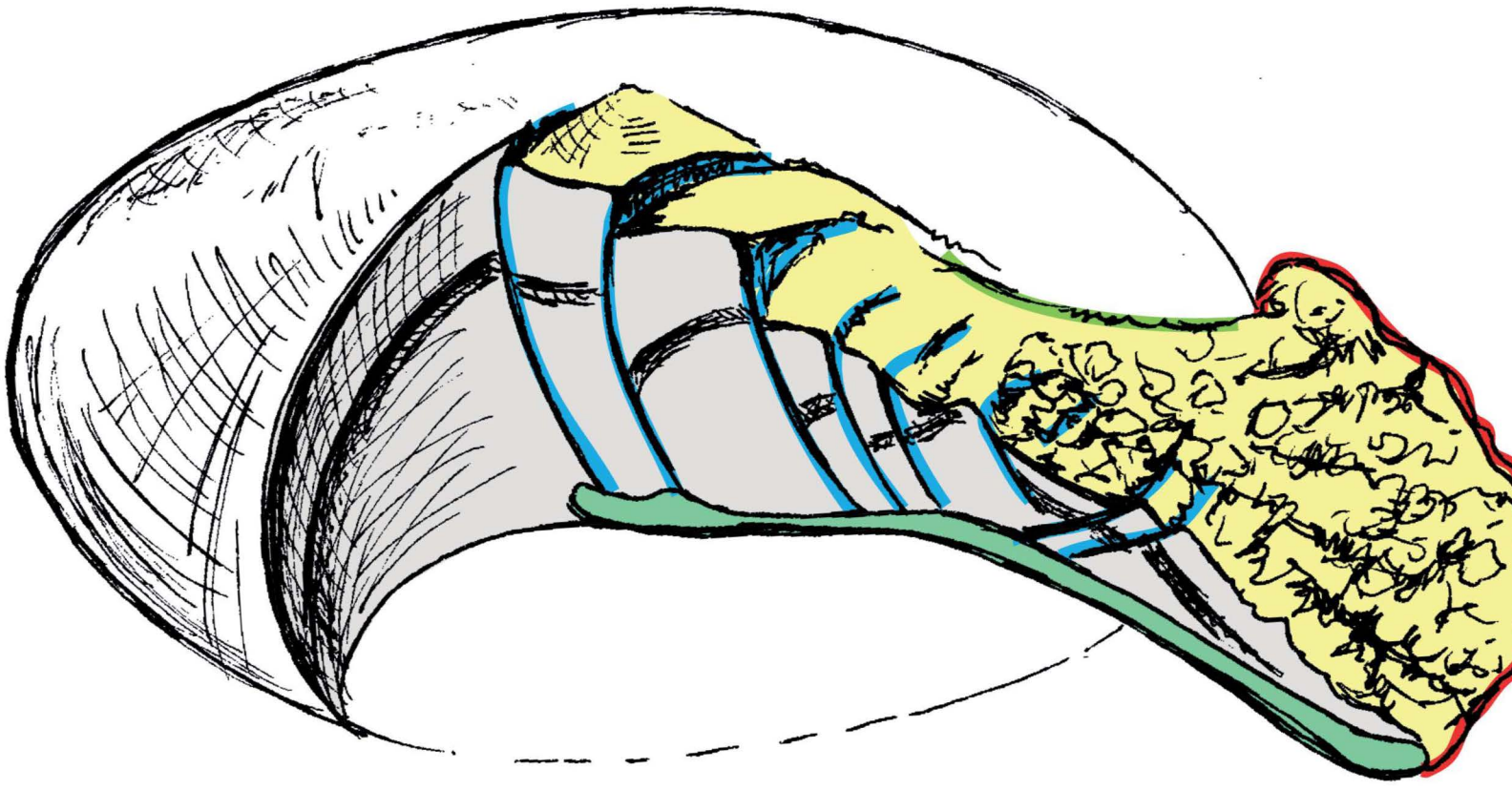

Figure 07